Journal of Organometallic Chemistry 694 (2009) 2786–2792

Contents lists available at ScienceDirect

Journal of Organometallic Chemistry

journal homepage: www.elsevier.com/locate/jorganchem

Preparation, luminescent, structural and electrical properties of Langmuir–Blodgett films of new organomercurial acetylide complex/heteropolyoxometalate hybrid composites

Li Liu [a,*], Jun Yang [a], Ling-Xiang Qiao [a], Ming Chen [a], Shi-Zhong Liu [a], Zu-Liang Du [b], Zheng-Ji Zhou [b], Wai-Yeung Wong [c,*]

[a] Ministry of Education Key Laboratory for the Synthesis and Application of Organic Functional Molecules and School of Chemistry and Chemical Engineering, Hubei University, Wuhan 430062, People's Republic of China
[b] Key Laboratory of Special Functional Materials, Henan University, Kaifeng 475001, People's Republic of China
[c] Department of Chemistry and Centre for Advanced Luminescence Materials, Hong Kong Baptist University, Waterloo Road, Kowloon Tong, Hong Kong, People's Republic of China

ARTICLE INFO

Article history:
Received 14 April 2009
Received in revised form 8 May 2009
Accepted 15 May 2009
Available online 21 May 2009

Keywords:
Crystal structure
Heteropolyacid
Fluorene
Mercury acetylide
Photoluminescence

ABSTRACT

A new family of organometallic/inorganic nanohybrid Langmuir–Blodgett (LB) films consisting of rigid-rod organomercury acetylide complex (OMA) as the π-conjugated organometallic composite and heteropolyacid salts MPA (MPA = $K_3PMo_{12}O_{40}$, $K_5BW_{12}O_{40}$, $Na_5IMo_6O_{62}$) of the Keggin and Anderson structures as the inorganic composite, were prepared and characterized by $\pi-A$ isotherms, UV–Vis absorption spectra, fluorescence spectra, scanning tunneling microscopy, atomic force microscopy imaging and low-angle X-ray diffraction. Our experimental results indicate that steady Langmuir and LB films are formed in pure water and heteropolyacid salt subphases. Luminescence spectra of hybrid LB films show that MPA can quench the emission of OMA to some extent. These alkynylmercury(II) based LB films display interesting electrical conductivity behavior. They all show decent electrical conductivity, and the tunneling current amounts to ±100 nA when the voltage is set at ±3 ~ ±5 V.

1. Introduction

The design, synthesis and structural characterization of new hybrid materials, of which many applications can be predicted, through the assembly of organic and inorganic building blocks, is a highly visible research area [1,2]. The construction of such organic–inorganic hybrid compounds has established new areas of research in the chemistry of materials that is based upon a bridge between inorganic and organic chemistry and is useful in order to obtain multifunctional materials which exhibit coexistence of solid-state magnetic, electric and/or optical properties [3,4]. In this field various strategies are being used with a common aim, i.e., to control the molecular assembly as far as possible, as it very often determines the solid-state properties of the material. Intermolecular interactions not only control the molecular assembly, but can exert a direct modulating influence on the molecular contributions to the material attributes which results in interesting cooperative effects.

An elegant approach to arrange molecules into well-organized multilayered films is the Langmuir–Blodgett (LB) technique [5–9]. It consists of a repetitive dipping of a solid substrate through a compressed monolayer onto the substrate, leading to a material with a precise thickness and a lamellar structure.

Polyoxometalates (POM) constitute a large class of inorganic compounds with remarkable chemical, structural, and electronic versatility that have applications in areas such as catalysis, medicine, and materials science [10–17]. In view of the ability of these molecular metal-oxide clusters to act as electronic acceptors and to accommodate transition metal centers in their structures, they have been used as inorganic components in the construction of hybrid organic–inorganic functional materials.

In this work, we explore the possibility of creating novel hybrid LB films that can combine two properties, one coming from the inorganic entities and the other from the organic part of the film. Thus, we have selected a group 12 mercury(II) acetylide derivative, which can introduce electronic delocalization within the LB film. They are expected to have functional potential as a component of luminescent film devices. With our growing interests in the design and synthesis of luminescent functional materials of groups 10–12 metallaynes [18–24], we report here a new example of the preparation of OMA/MPA hybrid LB films (MPA = $K_3PMo_{12}O_{40}$, $K_5BW_{12}O_{40}$ and $Na_5IMo_6O_{24}$, denoted as $KPMo_{12}$, KBW_{12} and $NaIMo_6$,

* Corresponding authors. Tel.: +86 27 62236098; fax: +86 27 88663043 (L. Liu), tel.: +852 34117074; fax: +852 34117348 (W.-Y. Wong).
E-mail addresses: liulihubei@gmail.com (L. Liu), rwywong@hkbu.edu.hk (W.-Y. Wong).

0022-328X/$ - see front matter © 2009 Elsevier B.V. All rights reserved.
doi:10.1016/j.jorganchem.2009.05.020

respectively) and their structures and electrical properties are discussed in detail.

2. Results and discussion

2.1. Synthesis, characterization and crystal structure analysis

The organometallic mercury complex OMA was prepared in good yield by the direct base-catalyzed mercuration of 2,7-diethynyl-9,9-dihexylfluorene with 2 equivalents of MeHgCl at room temperature according to the classical dehydrohalogenation procedures [25,26]. OMA is readily soluble in chlorinated solvents such as $CHCl_3$ and CH_2Cl_2 to give a pale yellow solution. The long hydrocarbon chains attached to the fluorene ring enhance the solubility of the complex.

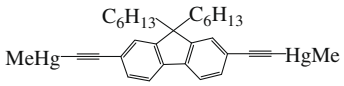

OMA

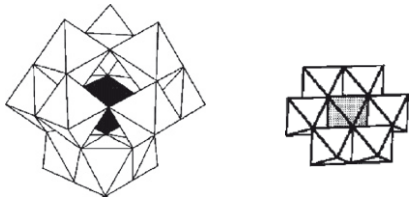

$K_3PMo_{12}O_{40}$ or $K_5BW_{12}O_{40}$ $Na_5IMo_6O_{24}$

Fig. 1. Molecular structure of compounds used in the construction of hybrid LB films.

The OMA complex displays weak IR ν(C≡C) absorptions at ca. 2124 cm^{-1}. The C≡C—H stretching mode in the starting material is absent. In the ^1H NMR spectra, the proton signals arising from the aromatic and other organic groups were observed. The symmetrical nature of OMA was evident from the NMR spectral pattern.

The molecular structure of OMA is depicted in Fig. 2a and some important bond distances and angles are given in Table 1. There are four structurally similar but independent molecules per asymmetric unit of the unit cell. The crystal structure shows a binuclear molecule in which two MeHg(II) units are linked by a diacetylenic

Table 1
Selected bond lengths (Å) and angles (°) for OMA.

	Molecule 1	Molecule 2	Molecule 3	Molecule 4
Hg(1)–C(1)	2.06(1)	2.04(1)	1.99(2)	1.85(2)
Hg(1)–C(2)	2.04(2)	2.06(2)	2.08(2)	2.00(2)
C(2)–C(3)	1.22(2)	1.17(2)	1.19(2)	1.19(2)
Hg(2)–C(19)	1.95(2)	2.07(1)	2.12(1)	2.07(1)
Hg(2)–C(18)	2.03(2)	2.11(2)	2.08(2)	2.05(2)
C(17)–C(18)	1.16(2)	1.15(2)	1.17(2)	1.23(2)
C(1)–Hg(2)–C(2)	176.8(6)	175.4(9)	175.8(7)	177.2(7)
Hg(1)–C(2)–C(3)	174(1)	174(2)	172(1)	178(2)
C(19)–Hg(2)–C(18)	175.5(7)	178.4(8)	175.4(7)	177.7(6)
Hg(2)–C(18)–C(17)	178(2)	171(2)	174(2)	171(1)

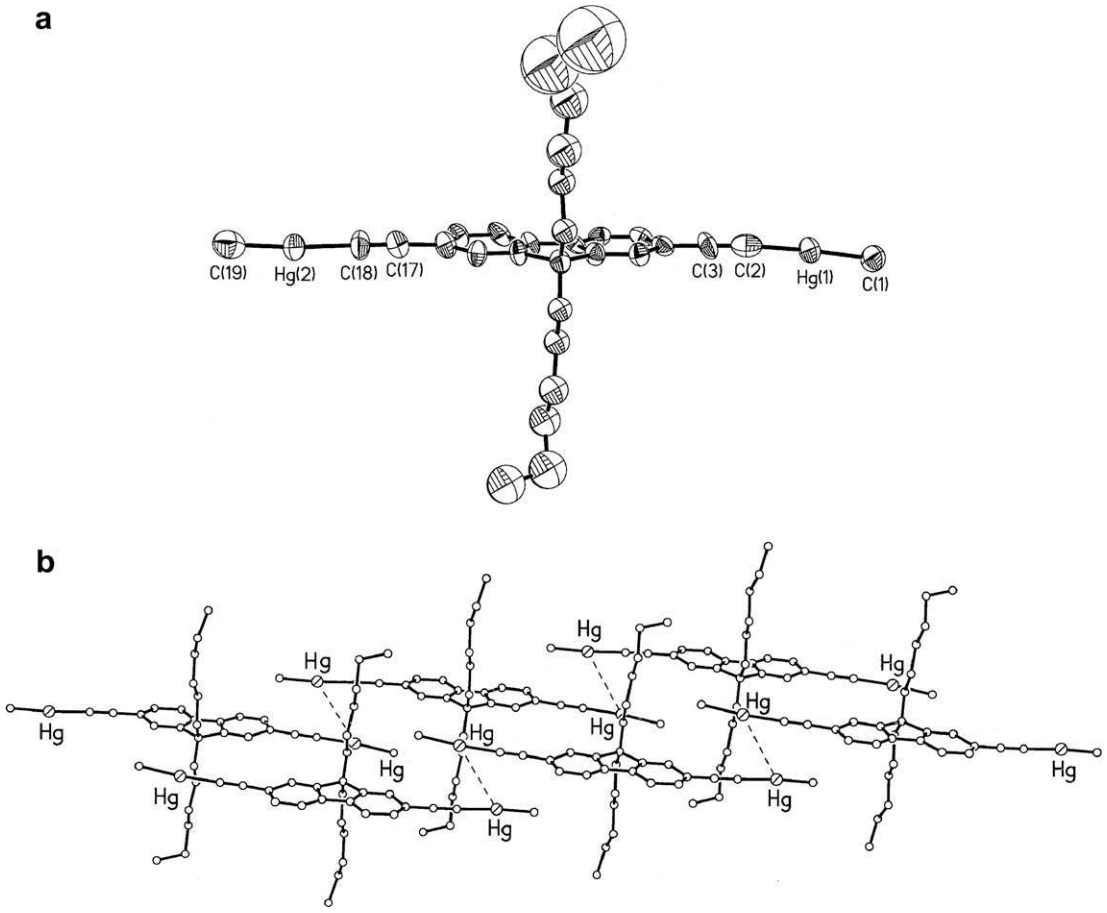

Fig. 2. (a) A perspective drawing of OMA and (b) the crystal packing showing the existence of mercurophilic interactions.

9,9-dihexylfluorene-2,7-diyl moiety in a rigid-rod manner. There is no apparent short intermolecular interactions between the fluorenyl rings as well as the Hg(II) centers. The mean Hg—C(alkyne) bond [Hg(1)—C(2) ~ 2.05(2) Å, Hg(2)—C(18) ~ 2.07(2) Å] is slightly longer than the Au—C(alkyne) bond in the gold(I) counterpart [25] but comparable to other Hg(II) acetylide compounds [24]. The fluorenediyl unit does not deviate significantly from planarity and the C≡C bonds in the ethynyl bridge are fairly typical at 1.15(2)–1.23(2) Å, fairly typical of metal–alkynyl σ-bonding. By virtue of the fact that $[MeHg]^+$ is isoelectronic and isolobal with the $[(PPh_3)Au]^+$ fragment, the MeHg—C≡C entity displays similar structural motifs and geometry in OMA with the gold(I) analog [24,25] and the angles C—Hg—C and Hg—C—C are close to linearity. Interestingly, examination of the crystal packing diagram for OMA reveals the involvement of ligand-unsupported mercurophilicity in its structure. There is a strong tendency for the molecules to aggregate together and the whole lattice structure is fully supported and stabilized by extensive non-covalent d^{10}–d^{10} Hg···Hg interactive vectors (ca. 4.037–4.039 Å) that link up the individual molecules in an organized network (Fig. 2b). While the Hg···Hg contacts here indicate that each of the individual interactions is relatively weak in nature, it is the large number of them that play a supramolecular role and generate a significant driving force for the observation of solid-state aggregation. We conceive that such mercurophilic forces are more than just van der Waals interactions in the present system [24,27–29], and can be compared to those of 3.71–4.25 Å for mononuclear $[Hg(C{\equiv}CR)_2]$ (R = Ph, $SiMe_3$) [30], 3.738–4.183 Å for binuclear [MeHgC≡CRC≡CHgMe] (R = 9,9-dioctylfluorenediyl and oligothienyl) [31,32] and 4.077 and 4.449 Å computed for molecular $(HgH_2)_n$ clusters (n = 2, 3) [33] and are toward the upper limit of those accepted as representing metallophilic interactions. This structure is unique in that no apparent weak Hg···η^2—C≡C interactions are observed which have been shown to be an important driving force for the solid-state aggregation process to take place in alkynyl complexes of Cu(I), Ag(I) and Hg(II) [34–37].

2.2. Surface pressure–area isotherms

Fig. 3 shows the surface pressure–area (π–A) isotherms of OMA on MPA and the pure water subphase solutions at 20 °C. The results show that they can form stable monolayer Langmuir film at the air–liquid interface even without the use of an auxiliary film-forming agent. The molecular area of OMA on the MPA aqueous solutions and pure water can be estimated by extrapolating the line part of π–A isotherm to the abscissa. The relevant data are displayed in Table 2. The isotherm is progressively modified by using different MPA polyoxoacids. For OMA film spreaded on the pure water subphase, for instance, the limiting area per molecule is 0.33 nm^2, whereas that of OMA in MPA aqueous subphase is 1.00–1.66 nm^2. The collapse pressure of OMA in $KPMo_{12}$ and Na_5I-Mo_6 aqueous solutions is 51.9–64.2 mN m^{-1}, larger than that in water phase (45.7 mN m^{-1}). It was shown that the LB films of OMA tend to be more stable as the length of alkyl chains on fluorene ring decreases from C_8 to C_6 (collapse pressure ~ 45.7 versus 23.2 mN m^{-1} for C_6- and C_8-based OMA with water, respectively). Apparently, isotherms on MPA aqueous solutions exhibited an increase in the molecular area compared with the case for pure water, suggesting that MPA molecules are not embedded inside the OMA.

Table 2
Surface pressure–area isotherm data of the LB films.

Film	Cross section (nm^2 $molecule^{-1}$)	Collapse pressure (mN m^{-1})
OMA/H_2O	0.33	45.7
OMA/KBW_{12}	1.00	34.1
OMA/$KPMo_{12}$	1.10	51.9
OMA/$NaIMo_6$	1.66	64.2

2.3. UV–Vis spectroscopy of LB films

OMA/MPA of multilayers (13 layers) as well as OMA/H_2O of 13 layers LB films of high morphological stability was successfully deposited onto quartz substrates by the vertical method. The transfer ratio was almost unity in both dipping and lifting processes, indicating the formation of Y-type LB films. As shown in Fig. 4, OMA/H_2O and OMA/MPA films display strong absorption bands in the near UV region. These bands are mainly associated with the organic $^1(\pi$–$\pi^*)$ transitions, possibly with some admixture of mercury atom orbitals, and the 0–0 absorption peak is assigned as the $S_0 \rightarrow S_1$ transition [31,38,39]. For OMA/MPA hybrids, the LB films exhibit intense peaks similar to OMA/H_2O which might cover the absorption peaks from the MPA [26]. Compared with OMA/H_2O, the absorption peaks of OMA/MPA LB films are slightly red shifted which are presumably due to the delocalized π-conjugation caused by OMA and MPA (see Table 3).

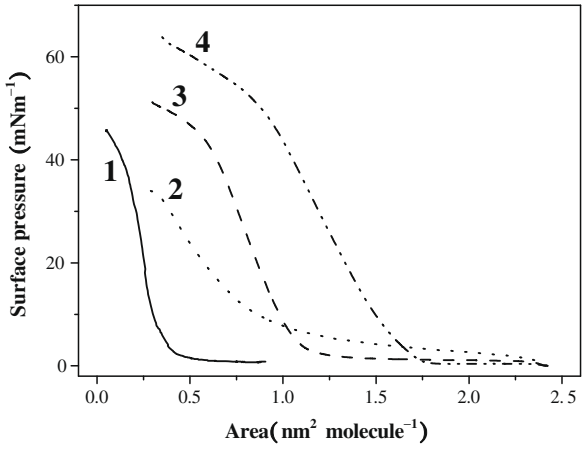

Fig. 3. Surface pressure–area (π–A) isotherms of monolayer films of (1) OMA/H_2O, (2) OMA/KBW_{12}, (3) OMA/$KPMo_{12}$ and (4) OMA/$NaIMo_6$.

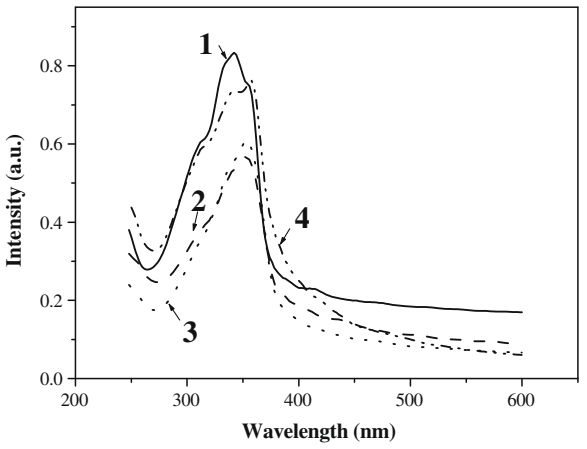

Fig. 4. UV–Vis spectra of LB films of OMA (13 layers) in (1) H_2O, (2) $KPMo_{12}$ (3) KBW_{12} (4) $NaIMo_6$.

Table 3
Absorption data for the LB films.

LB film	λ_{max} (nm)
OMA/H_2O	316*, 334*, 344, 356*, 414*
OMA/$KPMo_{12}$	316*, 340*, 353, 430*
OMA/KBW_{12}	316*, 342*, 354, 420*
OMA/$NaIMo_6$	316*, 344, 358, 418*

* It indicates a shoulder or weak peak.

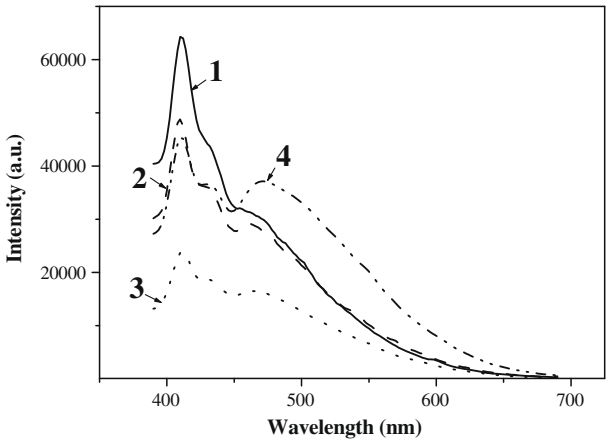

Fig. 5. PL spectra of 13-layer LB films of (1) OMA/H_2O, (2) OMA/$KPMo_{12}$, (3) OMA/KBW_{12} and (4) OMA/$NaIMo_6$.

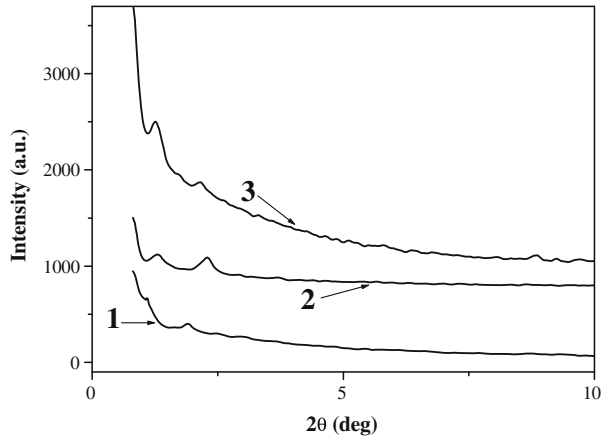

Fig. 6. Low-angle X-ray diffraction pattern of the as-prepared films of OMA in (1) $KPMo_{12}$ (2) $NaIMo_6$ (3) KBW_{12} deposited on glass.

2.4. Photoluminescence properties of LB films

The photoluminescence (PL) spectra of the LB films (13 layers) deposited on quartz were measured, with the excitation wavelength at 360 nm (Fig. 5). We observe broad intraligand-based $^1(\pi-\pi^*)$ emission peaks in the visible region in the range of 410–466 nm for each of them which arise from a singlet excited state (S_1) but no triplet emission was observed under ambient conditions. The luminescence is attributed to the organometallic part and its intensity decreased after formation of the hybrid LB films. The fluorescence emission patterns of 4 types of the films appear similar at room temperature. Interestingly, inclusion of MPA within the LB films causes notable changes in their luminescence properties compared with those observed on pure water. For hybrid LB films of OMA/$KPMo_{12}$ and OMA/KBW_{12}, the PL intensity at ~410 nm is lower than that of the OMA/H_2O system and it is found that MPA quenches the luminescence of OMA to a certain extent presumably by accepting the excited electrons [40]. However, for hybrid LB films of OMA/$NaIMo_6$, the PL intensity for the lower energy peak (>452 nm) is higher than that of the OMA/H_2O system, suggesting that MPA can facilitate aggregate emission bands and the aggregation is more intense in the hybrid LB films which usually quenches the fluorescence.

2.5. Low-angle X-ray diffraction

Correlation of molecular organization in crystals and in ultrathin films is of fundamental interest in the design of molecular materials based on thin films. Properties of molecular materials are critically dependent on the organization of the molecular building blocks. Take OMA as an example, two strong Bragg peaks are clearly identified in the X-ray diffractogram of 13-layer OMA/$KPMo_{12}$, OMA/KBW_{12} and OMA/$NaIMo_6$ LB films (Fig. 6). The highest peak of hybrid LB films for OMA/$KPMo_{12}$, OMA/KBW_{12} and OMA/$NaIMo_6$ at 1.09, 1.27 and 1.31 (2θ) corresponds to the {0 0 1} reflection, revealing a highly ordered stacking of different layers. According to the Bragg diffraction formula, $n\lambda = 2d\sin\theta$, we can calculate the monolayer average thickness $d/2$ for OMA/$KPMo_{12}$, OMA/KBW_{12} and OMA/$NaIMo_6$ to be 4.05, 3.48 and 3.37 nm, respectively. The periodicity of the layered structure deduced from this experiment is ca. 8.10, 6.96 and 6.74 nm, respectively.

2.6. Atomic force microscopy

Surface characterization of the LB films by atomic force microscopy (AFM) has also been performed. The image and structure of

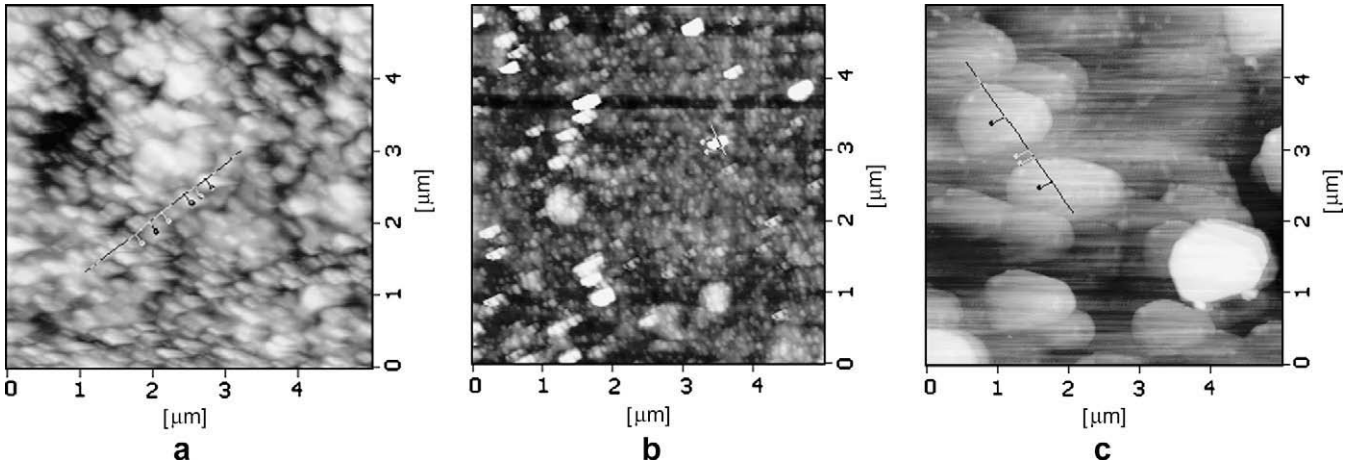

Fig. 7. AFM topography images of the (a) OMA/KBW_{12} monolayer film, (b) OMA/$KPMo_{12}$ monolayer film and (c) OMA/$NaIMo_6$ monolayer film.

the hybrid monolayer film deposited on mica was measured (Fig. 7). The topographic images of OMA/KBW_{12} (Fig. 7a) show that the hybrid LB film consists of disperse particles with different domain sizes of ca. 197–400 nm. OMA/KBW_{12} has an average surface roughness (*R*a) of 5.5 nm and the largest roughness (*R*z) is 66.8 nm. A dimensionally split phase structure can be observed in which the darker area is mostly filled with MPA and the higher and brighter area is mostly filled with OMA [42]. The topographic images of OMA/$KPMo_{12}$ and OMA/$NaIMo_6$ monolayer films are shown in Fig. 7b and c with the *R*a values of 1.0, 7.7 nm and *R*z of 16.4, 40.5 nm, respectively.

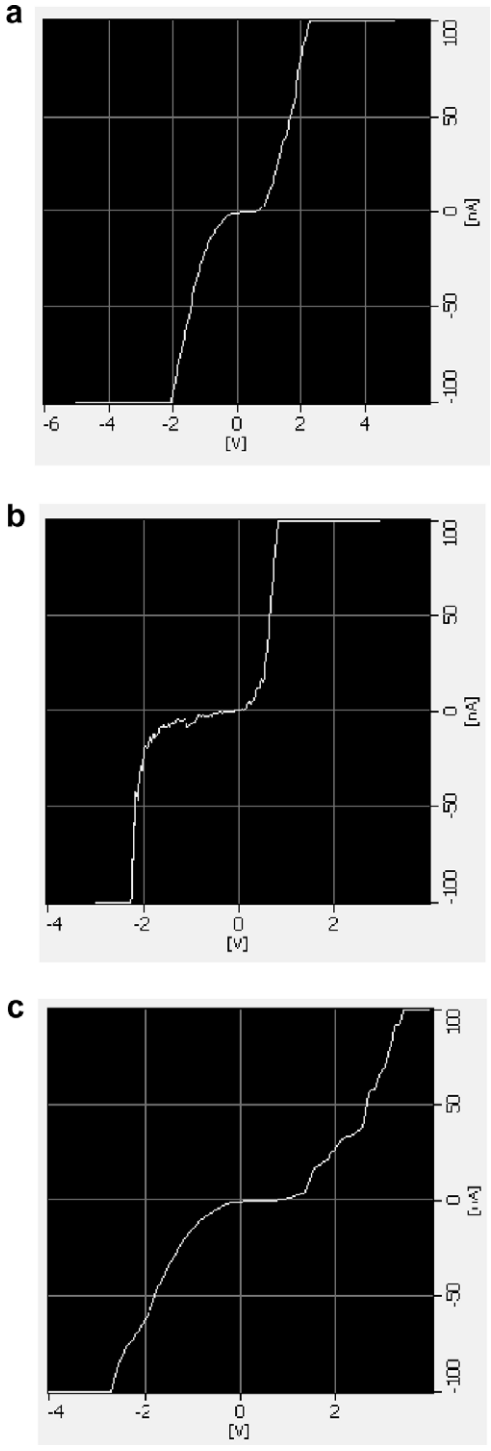

Fig. 8. The *I–V* curve of a monolayer film on the silica wafer for (a) OMA/KBW_{12} (b) OMA/$KPMo_{12}$ and (c) OMA/$NaIMo_6$.

2.7. Electrical characterization of monolayer LB films by scanning tunneling microscopy

In our preliminary experiments, the electrical conductivity behavior of OMA/$KPMo_{12}$, OMA/KBW_{12} and OMA/$NaIMo_6$ monolayer films on silica wafer was examined using scanning tunneling microscopy. Saliently, they can show good electrical conductivities and representative *I–V* plots are shown in Fig. 8 for the devices. The tunneling current for the OMA/KBW_{12}, OMA/$KPMo_{12}$ and OMA/$NaIMo_6$ films amounts to ±100 nA when the voltage is set at ±5, ±3 and ±4 V, respectively. While pure mercury(II) diynes and polyynes are generally very poor conductors in the intrinsic state, our hybrid LB composites in the device can be made to be semiconducting. We anticipate that the device performance would be enhanced when the quality of the prepared thin films can be further improved [41].

3. Concluding remarks

The combination of mercury(II) diyne functionalized with 9,9-dialkylated fluorene chromophore with various heteropolyacid salts (MPA) provides an effective approach for the exploration of new organometallic/MPA structures in LB films which would be useful for different opto- and photo-electric applications. These materials can form steady monolayers and multilayers at the interface of air and MPA aqueous solutions without the use of an auxiliary film-forming agent, and the stability of LB films is shown to be dependent of the alkyl chain length. Because of the charge transfer between mercury acetylide donor and heteropolyacid salt acceptor as well as the possible hydrogen-bonding network formation and adsorption phenomenon, the films can be significantly compressed and aggregated in the solid region and Y-type nanohybrid LB films can be prepared. Organomercury acetylides permits a delocalized electron transfer in the π-conjugated bond system, and can be made electrically conductive to deposition by mixing with film forming MPA in the LB films. For the hybrid LB films based on OMA, weak $d^{10}\cdots d^{10}$ mercurophilic interaction, strong $\pi-\pi^*$ transition between the alkyne bond of OMA and the ligand aromatic system, and electron transfer between electron donor and acceptor are believed to be the critical driving forces for the observable electrical conducting effect of these hybrid LB films. Such an organometallic/inorganic multifunctional assembly can afford new ultrathin materials. We envision that the work can be further extended to different kinds of polyoxometalate clusters, possibly producing new inorganic/organometallic composite materials and these LB films may open up a fascinating study on realizing practical molecular devices with specific optoelectronic functional properties.

4. Experimental section

4.1. General procedures

Solvents were carefully dried and distilled from appropriate drying agents prior to use. Commercially available reagents were used without further purification unless otherwise stated. Three types of MPA, viz. $K_3PMo_{12}O_{40}$, $K_5BW_{12}O_{40}$ and $Na_5IMo_6O_{24}$ (denoted as $KPMo_{12}$, KBW_{12} and $NaIMo_6$ respectively) were synthesised according to the procedures previously reported [13]. Infrared spectra were recorded as CH_2Cl_2 solutions using a Perkin-Elmer Paragon 1000 PC or Nicolet Magna 550 Series II FTIR spectrometer, using CaF_2 cells with a 0.5 mm path length. Fast atom bombardment (FAB) mass spectra were recorded on a Finnigan MAT SSQ710 system. NMR spectra were measured in $CDCl_3$ on a Varian Inova 400 MHz FT-NMR spectrometer and chemical shifts

are quoted relative to tetramethylsilane for ^{1}H and ^{13}C nuclei and H_3PO_4 for ^{31}P nucleus. Ultraviolet–Visible (UV–Vis) spectra were measured on a UNICAM Heλios α spectrometer. Low-angle X-ray diffraction measurements were carried out on a Philips X'pert Pro instrument, operating with a monochromated Cu Kα radiation source at 40 kV and 50 mA. Photoluminescence spectra were recorded on a SPEX F212 fluorescence spectrometer. AFM image and scanning tunneling microscopy of the LB films were measured on a SPA-400 atomic force microscope.

4.2. Synthesis of OMA

The diethynyl ligand (15.3 mg, 0.04 mmol) in THF (5 mL) was first combined with MeHgCl (20.1 mg, 0.08 mmol) in MeOH (15 mL) and 0.2 M basic MeOH (4 mL) was subsequently added to give a pale yellow suspension. The solvents were then decanted and the light yellow solid of OMA (29.2 mg, 90%) was air-dried. IR (KBr): ν(C≡C) 2124 cm^{-1}. ^{1}H NMR ($CDCl_3$): δ 7.57 (m, 2H, $H_{1,8}$), 7.43 (m, 4H, $H_{3,4,5,6}$), 1.92 (m, 4H, $CH_2(CH_2)_4CH_3$), 1.12–0.96 (m, 12H, $CH_2(CH_2)_3CH_2CH_3$), 0.76 (t, J = 7.2 Hz, 6H, $(CH_2)_5CH_3$), 0.72 (s, 6H, Me), 0.54 (m, 4H, $CH_2(CH_2)_3CH_2CH_3$). FAB–MS: m/z 811 [M^+]. Anal. Calc. for $C_{31}H_{38}Hg_2$: C, 45.86; H, 4.72. Found: C, 45.55; H, 4.50.

4.3. Monolayer and LB film fabrication

The formulae of the composites for the LB films are shown in Fig. 1. MPA can be organized as monolayers using the LB technique. Monolayer formation and deposition were carried out on a French LB 105 slot under room temperature condition at 20 ± 1 °C. The surface pressure was measured by the Wilhelmy method. Triple-distilled deionized water (pH 6) was used as the subphase. The spreading solution of OMA (1×10^{-4} mmol dm^{-3}) in chloroform was spread onto the pure water subphase using a microsyringe; when the solvent had evaporated thoroughly, compression began with the compression rate at 10 cm^2 min^{-1} and the curve was recorded. The procedure of LB film fabrication was essentially the same as for the monolayer except that the subphase is MPA aqueous solution (1×10^{-6} mol L^{-1}). All the experiments for monolayer deposition were performed under a surface pressure of 25 mN m^{-1}. In the case where a stable Langmuir monolayer of OMA was formed on the subphase, the monolayer was subsequently deposited onto ITO or quartz substrates by the vertical dipping method at a rate of 3 mm min^{-1}, resulting in a fairly good deposition of a typical Y-mode film. The number of layers of LB film prepared here is equal to the number of dipping or lifting processes, on each of which a floating Langmuir monolayer was transferred onto the substrate with a good transfer ratio.

5. X-ray crystallography

Crystals suitable for X-ray diffraction studies were grown by slow evaporation of each of the respective solutions in CH_2Cl_2/hexane at room temperature. Geometric and intensity data were collected at 293 K using graphite-monochromated Mo Kα radiation (λ = 0.71073 Å) on a Bruker Axs SMART 1000 CCD diffractometer. The crystallinity, orientation matrix, and accurate unit-cell parameters were determined according to standard procedures. The collected frames were processed with the software SAINT [43] and an absorption correction (SADABS) [44] was applied to the collected reflections. The structure was solved by the Direct or Patterson methods (SHELXTL) [45] in conjunction with standard difference Fourier techniques and subsequently refined by full-matrix least-squares analyses on F^2. Hydrogen atoms were generated in their idealized positions and all non-hydrogen atoms were assigned with anisotropic displacement parameters. Crystal data for OMA: $C_{31}H_{38}Hg_2$, M_w = 811.79, monoclinic, space group $P\bar{1}$, a = 14.2680 (7), b = 21.739(1), c = 21.749(1) Å, α = 83.8330(1), β = 70.829(1), γ = 70.861(1)°, V = 6019.8(5) $Å^3$, Z = 8, ρ_{calc} = 1.791 Mg m^{-3}, μ(Mo Kα) = 10.204 mm^{-1}, F(0 0 0) = 3072, T = 293 K. 30,264 reflections measured, of which 20,828 were unique (R_{int} = 0.0554). Final R_1 = 0.0670 and wR_2 = 0.1542 for 7000 observed reflections with $I > 2\sigma(I)$.

Supplementary material

CCDC 726662 contains the supplementary crystallographic data for this paper. These data can be obtained free of charge from the Cambridge Crystallographic Data Centre via www.ccdc.cam.ac.uk/data_request/cif.

Acknowledgements

The authors acknowledge the financial support from National Natural Science foundation of China (20671033) and the Excellent Mid-youth Creative Team Project of Hubei Province Education Office (T200701). W.-Y.W. thanks the Hong Kong Research Grants Council (HKBU202508) and the Hong Kong Baptist University (FRG/07-08/II-65) for financial support.

References

[1] J.P. Hargmann, D. Hargmann, J. Zubieta, Angew. Chem., Int. Ed. 38 (1999) 2638.
[2] T. Ito, H. Yashiro, T. Yamase, Langmuir 22 (2006) 2806.
[3] K. Awaga, E. Coronado, M. Drillon, MRS Bull. (2000) 52.
[4] A.E. Coronado, J.R. Galán-Mascarós, C.J. Gómez-García, V.L. Lauhkin, Nature 408 (2000) 447.
[5] G. Roberts (Ed.), Langmuir–Blodgett Films, Plenum, New York, 1990.
[6] A. Ulman, An Introduction to Ultrathin Organic Films: From Langmuir–Blodgett to Self-Assembly, Academic Press, Boston, 1991.
[7] D.R. Talham, Chem. Rev. 104 (2004) 5479.
[8] H. Kuhn, D. Möbius, H. Bücher, Physical Methods of Chemistry, Part IIIB, Wiley-Interscience, New York, 1972 (Chapter VII).
[9] G.L. Gaines Jr., Insoluble Monolayers at Liquid–Gas Interface, Wiley-Interscience, New York, 1966.
[10] Thematic Issue on Polyoxometalates, Chem. Rev. 98 (1998) 1–388.
[11] T. Yamase, M.T. Pope (Eds.), Polyoxometalate Chemistry for Nano-composite Design, Kluwer Academic/Plenum Publishers, New York, 2002.
[12] M.T. Pope, Heteropoly and Isopoly Oxometalates, Berlin, Springer, 1983.
[13] M.T. Pope, A. Müller (Eds.), Polyoxometalate Chemistry: From Topology Via Self-Assembly to Applications, Kluwer, Dordrecht, The Netherlands, 2001.
[14] J.J. Borrás-Almenar, E. Coronado, A. Müller, M.T. Pope (Eds.), Polyoxometalate Molecular Science, Kluwer, Dordrecht, The Netherlands, 2001.
[15] V.W. Day, W.G. Klemperer, Science 228 (1985) 533.
[16] T. Okuhara, N. Mizuno, M. Misono, Adv. Catal. 41 (1996) 113.
[17] M.T. Pope, A. Müller, Angew. Chem., Int. Ed. Engl. 30 (1991) 34.
[18] L. Liu, W.-Y. Wong, S.-Y. Poon, J.-X. Shi, K.-W. Cheah, Z.-Y. Lin, Chem. Mater. 18 (2006) 1369.
[19] L. Liu, Y.-W. Lam, W.-Y. Wong, J. Organomet. Chem. 691 (2006) 1092.
[20] L. Liu, W.-Y. Wong, J.-X. Shi, K.-W. Cheah, T.-H. Lee, M.-L. Leung, J. Organomet. Chem. 691 (2006) 4028.
[21] L. Liu, W.-Y. Wong, C.-L. Ho, Aust. J. Chem. 59 (2006) 434.
[22] L. Liu, W.-Y. Wong, J.-X. Shi, K.-W. Cheah, J. Polym. Sci. A: Polym. Chem. 44 (2006) 5588.
[23] L. Liu, S.-Y. Poon, W.-Y. Wong, J. Organomet. Chem. 690 (2005) 5036.
[24] W.-Y. Wong, Coord. Chem. Rev. 251 (2007) 2400.
[25] W.-Y. Wong, K.-H. Choi, G.-L. Lu, J.-X. Shi, P.-Y. Lai, S.-M. Chan, Z. Lin Organometallics 20 (2001) 5446.
[26] E.-B. Wang, C.-W. Hu, L. Xu, An Introduction to Heteropolyacid, Chemical Engineering Press, New York, 1998.
[27] P. Pyykko, Chem. Rev. 97 (1997) 597 (and references cited therein).
[28] S.S. Batsanov, J. Chem. Soc., Dalton Trans. (1998) 1541.
[29] A. Bondi, J. Phys. Chem. 68 (1964) 441.
[30] S.J. Faville, W. Henderson, T.J. Mathieson, B.K. Nicholson, J. Organomet. Chem. 580 (1999) 363.
[31] B.-B. Xu, Y.-G. Wei, C.-L. Barnes, Z.-H. Peng, Angew. Chem., Int. Ed. 40 (2001) 2290.
[32] W.-Y. Wong, K.-H. Choi, G.-L. Lu, Z. Lin, Organometallics 21 (2002) 4475.
[33] X. Wang, L. Andrews, Inorg. Chem. 43 (2004) 7146.
[34] W.-Y. Wong, G.-L. Lu, L. Liu, J.-X. Shi, Z. Lin, Eur. J. Inorg. Chem. (2004) 2066.
[35] D. Rais, D.M.P. Mingos, R. Vilar, A.J.P. White, D.J. Williams, Organometallics 19 (2000) 5209.

[36] P.W.R. Corfield, H.M.M. Shearer, Acta Crystallogr. 20 (1966) 502.
[37] C. Brasse, P.R. Raithby, M.-A. Rennie, C.A. Russell, A. Steiner, D.S. Wright, Organometallics 15 (1996) 639.
[38] L. Liu, Z.-X. Chen, S.-Z. Liu, W.-Y. Wong, Acta Chim. Sinica 64 (2006) 884.
[39] L. Liu, M.-X. Li, W.-Y. Wong, Aust. J. Chem. 58 (2005) 799.
[40] W.-Y. Wong, L. Liu, J.-X. Shi, Angew. Chem., Int. Ed. 42 (2003) 4064.
[41] L. Liu, W.-H. Ai, M.-J. Li, S.-Z. Liu, C.-M. Zhang, H.-X. Yan, Z.-L. Du, W.-Y. Wong, Chem. Mater. 19 (2007) 1704.
[42] L. Liu, L.-X. Qiao, S.-Z. Liu, D.-M. Cui, C.-M. Zhang, Z.-J. Zhou, W.-Y. Wong, J. Polym. Sci. Part A: Polym. Chem. 46 (2008) 3193.
[43] SAINT+, ver. 6.02a, Bruker, Analytical X-ray System, Inc., Madison, WI, 1998.
[44] G.M. Sheldrick, SADABS, Empirical Absorption Correction Program, University of Göttingen, Germany, 1997.
[45] G.M. Sheldrick, SHELXTL™, Reference Manual, ver. 5.1, Madison, WI, 1997.